The Astronomical Journal, 150:87 (11pp), 2015 September doi:10.1088/0004-6256/150/3/87

THE HOST GALAXIES OF MICRO-JANSKY RADIO SOURCES

K. M. Luchsinger[1,2], M. Lacy[2], K. M. Jones[3], J. C. Mauduit[4], J. Pforr[5], J. A. Surace[4], M. Vaccari[6], D. Farrah[7], E. Gonzales-Solares[8], M. J. Jarvis[6,9], C. Maraston[10], L. Marchetti[11], S. Oliver[12], J. Afonso[13,14,15], D. Cappozi[10], and A. Sajina[16]

[1] St. Johns College, 60 College Avenue, Annapolis, MD 21401, USA
[2] National Radio Astronomy Observatory, 520 Edgemont Road, Charlottesville, VA 22903, USA
[3] Department of Astronomy, University of Virginia, 530 McCormick Road, Charlottesville, VA 22904, USA
[4] Spitzer Science Center, California Institute of Technology, Pasadena, CA 91125, USA
[5] Laboratoire dAstrophysique de Marseille, 38, rue Frédéric Joliot-Curie, F-13388 Marseille cedex 13, France
[6] Physics Department, University of the Western Cape, Private Bag X17, 7535, Bellville, Cape Town, South Africa
[7] Department of Physics, Virginia Tech, Blacksburg, VA 24061, USA
[8] Institute of Astronomy, Madingley Road, Cambridge CB3 0HA, UK
[9] Astrophysics, Department of Physics, Keble Road, Oxford OX1 3RH, UK
[10] Institute of Cosmology and Gravitation, Dennis Sciama Building, Burnaby Road, Portsmouth PO1 3FX, UK
[11] Department of Physical Sciences, The Open University, Milton Keynes, MK7 6AA, UK
[12] Astronomy Centre, Department of Physics and Astronomy, University of Sussex, Brighton, BN1 9QH, UK
[13] Observatorio Astronomico de Lisboa, Observatorio Astronomico de Lisboa, Portugal
[14] Instituto de Astrofísica e Ciências do Espaço, Universidade de Lisboa, OAL, Tapada da Ajuda, PT1349-018 Lisboa, Portugal
[15] Departamento de Física, Faculdade de Ciências, Universidade de Lisboa, Edifício C8, Campo Grande, PT1749-016 Lisbon, Portugal
[16] Department of Physics and Astronomy, Tufts University, 212 College Avenue, Medford, MA 02155, USA
Received 2014 November 16; accepted 2015 June 29; published 2015 August 25

ABSTRACT

We combine a deep 0.5 deg^2, 1.4 GHz deep radio survey in the Lockman Hole with infrared and optical data in the same field, including the *Spitzer* Extragalactic Representative Volume Survey (SERVS) and UKIDSS near-infrared surveys, to make the largest study to date of the host galaxies of radio sources with typical radio flux densities $\sim$50 μJy. 87% (1274/1467) of radio sources have identifications in SERVS to $AB \approx 23.1$ at 3.6 or 4.5μm, and 9% are blended with bright objects (mostly stars), leaving only 4% (59 objects), which are too faint to confidently identify in the near-infrared. We are able to estimate photometric redshifts for 68% of the radio sources. We use mid-infrared diagnostics to show that the source population consists of a mixture of star-forming galaxies, rapidly accreting (cold mode) active galactic nuclei (AGNs) and low accretion rate (hot mode) AGNs, with neither AGNs nor star-forming galaxies clearly dominating. We see the breakdown in the K–z relation in faint radio source samples, and show that it is due to radio source populations becoming dominated by sources with radio luminosities $\sim 10^{23}$ WHz^{-1}. At these luminosities, both the star-forming galaxies and the cold mode AGNs have hosts with stellar luminosities of about a factor of two lower than those of hot mode AGNs, which continue to reside in only the most massive hosts. We show that out to at least $z \sim 2$, galaxies with stellar masses $>10^{11.5}\,M_{\odot}$ have radio-loud fractions up to $\sim$30%. This is consistent with there being a sufficient number of radio sources for radio-mode feedback to play a role in galaxy evolution.

Key words: galaxies: active – galaxies: evolution – radio continuum: galaxies

1. INTRODUCTION

The radio source population at a 1.4 GHz flux density of $S_{1.4} < 1$ mJy contains a mixture of active galactic nuclei (AGNs), both radio-loud and radio-quiet, and star-forming galaxies (Condon 1992; Afonso et al. 2005; Simpson et al. 2006). Radio-loud AGNs have, historically, been easier to study, being three to four orders of magnitude more luminous in the radio than star-forming galaxies and dominating radio surveys at bright flux density levels. However, recent studies have shown that within populations with characteristic flux densities of tens to hundreds of micro-Janskys (hereafter the μJy population), the predominance of radio-loud AGNs gives way and the population begins to include significant numbers of radio-quiet AGNs and star-forming galaxies (Jarvis & Rawlings 2004; Simpson et al. 2006; Huynh et al. 2008; Seymour et al. 2008; Smolčić et al. 2008; Strazzullo et al. 2010; Mao et al. 2012; White et al. 2012; Bonzini et al. 2013). Characterizing this mixed population is important for using radio surveys to study the star formation history of the universe (Karim et al. 2011; Zwart et al. 2014), the cosmic history of AGN activity (Smolčić et al. 2015), and using radio continuum surveys for cosmological purposes.

Multiwavelength observations of radio sources allow the study of the relative distributions and properties of the three dominant types of sources (radio-loud AGNs, radio-quiet AGNs, and star-forming galaxies) among the various wavelengths. Previous studies have used this multiwavelength technique to examine radio source populations in several deep fields, but have reached differing results as to the contributions of the different galaxy types. Most studies suggest a significant fraction (Simpson et al. 2006; Huynh et al. 2008; Smolčić et al. 2008) or a majority (Seymour et al. 2008; Padovani et al. 2011, 2015; White et al. 2012) of star-forming and radio-quiet galaxies within the μJy population, though some authors argue a continuation of the dominance of radio-loud AGNs from the Jansky and milliJansky populations to sub-milli-Jansky levels (Mignano et al. 2008).

Deep radio surveys, combined with multiwavelength data, are essential for studying the nature of the host galaxies of the AGN-powered radio source population, and, because they are deep enough to contain a mixture of both radio-loud and radio-

quiet objects, are helpful in our understanding of the origin of radio-loudness in AGNs. At high 1.4 GHz radio luminosities ($L_{1.4} > 10^{24}$ WHz^{-1}) radio sources have long been known to be hosted by the most massive galaxies at all redshifts. Early work by Lilly & Longair (1984) and Lilly (1989) showed that the near-infrared K-band magnitudes of radio galaxies formed a tight Hubble diagram. This so-called "K–z relation" has been found to be a very useful tool for estimating the redshifts of distant, luminous radio sources, and is only very weakly dependent on radio luminosity for radio sources with $L_{1.4} \gtrsim 10^{24}$ Wm^{-2} (Willott et al. 2003; McLure et al. 2004). The scatter in the K–z relation toward fainter K-magnitudes has long been predicted to increase as fainter radio samples are studied, however (e.g., Jarvis et al. 2001), when radio source populations become dominated by progressively lower radio-luminosity AGNs and star-forming galaxies. The first signs of this breakdown in the K–z relation start to appear in μJy radio surveys (Simpson et al. 2012), which we confirm with a larger sample of sources in this paper.

Understanding the mixture of galaxies that host the μJy radio source population is essential for planning for future radio observatories such as the SKA, in particular, for cosmological studies where different types of host galaxies cluster differently (e.g., Ferramacho et al. 2014). We therefore decided to use some of the best currently available multiwavelength data to investigate the nature of the radio source host population. We base our multiwavelength catalog on the *Spitzer* Extragalactic Representative Volume Survey (SERVS), which uses deep *Spitzer* data to detect galaxies out to $z \sim 5$ (Mauduit et al. 2012). All five fields chosen by this survey were selected specifically to be integrated into multi-wavelength observations. In particular, the Lockman Hole field has two deep radio surveys within it, the very deep survey of Owen et al. (2009) in the north of the field and the wider, but somewhat shallower survey of Ibar et al. (2009) in the east. In this paper, we match the SERVS data with the Ibar et al. radio survey, and other surveys in the Lockman Hole field at optical through infrared wavelengths to investigate the host galaxy properties of the μJy radio source population. These data are summarized in Section 2. Details of the catalogs and band-matching are given in Section 3, and Section 4 discusses the quality of the photometric redshifts. The methodology for discriminating between AGNs and star-forming galaxies is presented in Section 4. Section 6 presents the properties of the radio sources, and conclusions may be found in Section 7. A cosmological model of $\Omega_M = 0.3$, $\Omega_\Lambda = 0.7$, and $H_0 = 70$ kms^{-1} Mpc^{-1} is assumed throughout the text.

2. MULTIWAVELENGTH OBSERVATIONS

The Lockman Hole is a particularly appealing candidate for a multiwavelength study because there have been many observations made of it in a wide variety of wavelengths. These data can be combined to form a very thorough study, encompassing objects with redshifts out as far as $z \approx 5$. We have assembled a multiwavength data set, detailed below, with which to study the host galaxies of μJy radio sources in this field. Figure 1 shows the spatial overlap of the data sets described below.

2.1. SERVS Data

SERVS uses deep *Spitzer* data taken during the postcryogenic *Spitzer* Space Telescope mission over the course of 1400 hr using the Infrared Array Camera (IRAC) at wavelengths of 3.6 and 4.5 μm, and detects objects out to $z \approx 5$. The survey covers a total of 18 deg^2 to a detection limit of $\approx$2 μJy ($AB = 23.1$) in five fields, including 4 deg^2 in the Lockman Hole. SERVS catalogs were produced using Sextractor (Bertin & Arnouts 1996) as detailed in Mauduit et al. (2012).

2.2. Optical Data

González-Solares et al. (2011) observed the Lockman Hole with the Isaac Newton Telescope Wide Field Camera in the u, g, r, i, and z bands, with AB magnitude limits of 23.9, 24.5, 24.0, 23.3, and 22.0, respectively. Supplementary observations were taken with the Mosaic 1 camera on the Mayall 4 m Telescope of the Kitt Peak National Observatory in the g, r, and i bands. Details of the source extraction are given in González-Solares et al. (2011).

2.3. Ground-based Near-infrared Data

The UKIRT Infrared Deep Sky Survey (UKIDSS) observed the Lockman Hole as part of its Deep Extragalactic Survey using the Wide Field Camera (WFCAM) of the United Kingdom Infrared Telescope (UKIRT) at wavelengths of 1.2 and 2.2 μm, corresponding to the J and K bands, respectively. The survey reaches AB magnitude depths of $J_{AB} = 23.1$ and $K_{AB} = 22.5$. Lawrence et al. (2007) describe the survey and the production of the catalogs.

2.4. Spitzer Wide-area Infrared Extragalactic (SWIRE) Data

The SWIRE survey observed the Lockman Hole during its cryogenic mission using the IRAC and the Multiband Imaging Photometer for *Spitzer* (MIPS). IRAC observed the Lockman Hole using all four channels, 3.6, 4.5, 5.8, and 8.0 μm; and MIPS observed the Lockman Hole with all three of its channels, 24, 70, and 160 μm. The SWIRE catalogs reach depths of $\approx$10 μJy ($AB \approx 21.4$) at 3.6 and 4.5 μm. SWIRE detected galaxies out to $z \approx 3$ (Lonsdale et al. 2003). Details of the data release used may be found in the SWIRE data release 2 document.[16]

2.5. Radio Data

Part of the Lockman Hole was observed at frequencies of 610 MHz and 1.4 GHz using the Giant Metre-wave Radio Telescope (GMRT) and the Very Large Array (VLA), respectively, by Ibar et al. (2009). Their survey covered $\approx$0.5 deg^2 in the southern region of the Lockman Hole (centered on R.A., decl. 163°.0, 57°.35, generally called the "Lockman Hole East") and contains 1452 radio sources detected at 1.4 GHz, comprised of 1467 discrete components. The GMRT data reach an rms noise of $\approx$15 μJy beam^{-1}, and the VLA data an rms of $\approx$6 μJy beam^{-1} in the center of the surveys, where the sensitivity is highest, tapering off to $\approx$10 μJy beam^{-1} at 1.4 GHz toward the edge of the survey region (see Figure 2 for the flux density distribution). The depth of the GMRT data is

[16] http://irsa.ipac.caltech.edu/data/SPITZER/SWIRE/docs/delivery_doc_r2_v2.pdf

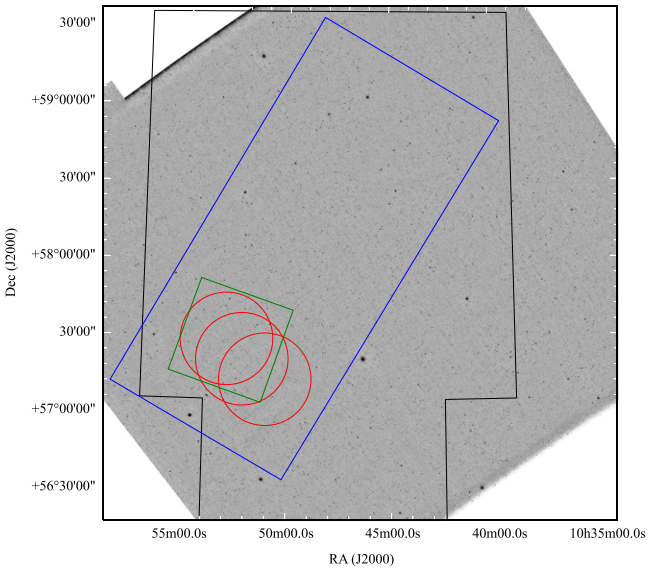

Figure 1. Surveys in the Lockman Hole used in this work. The grayscale shows the SWIRE 24 μm image, which is close to coincident with both the IRAC SWIRE coverage, and the optical imaging survey of González-Solares et al. (2011). The black outline shows the coverage of the UKIDSS DXS survey, the blue outline shows the SERVS coverage and the red circles show the positions of the VLA pointings used for the Ibar et al. (2009) radio survey. The green square shows the deep ("level 3") Herschel HerMES coverage (the whole field is covered to a lower depth), see Section 5.5.

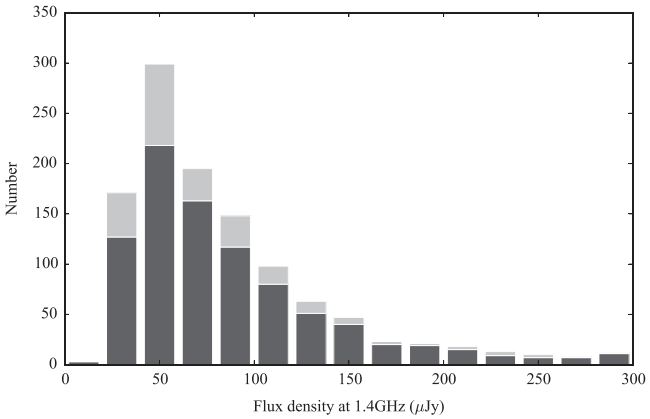

Figure 2. Histogram of flux densities at 1.4 GHz for our sample. The dark gray indicates objects with $\geqslant$4-band photometric redshifts, the lighter gray objects lacking photometric redshifts.

such that nearly all of the 1.4 GHz sources have counterparts at 610 MHz.

3. CATALOG MATCHING

Data from the optical through far-infrared surveys were combined into a SERVS "Data Fusion" catalog[17], using a matching radius of 1.″0 to match them to the SERVS dual-band catalog. This catalog contained 951102 objects covering the full 4 deg^2 of the SERVS Lockman area. Details of this catalog will be presented in M. Vaccari et al. (2015, in preparation). This Fusion catalog was then matched to the 1467 individual component detections at 1.4 GHz (with a peak-to-noise ratio >5) in the Ibar et al. (2009) catalog. The radio sources were matched to the SERVS Fusion catalog using a selection radius of 1.2 arcsec (compared to a 4 arcsec beamsize), which resulted in 1245 matched objects—an 85% match rate down to the $AB \approx 23.1$ catalog limit. We then compared the remaining 222 unmatched radio components with the SERVS data manually, and matched an additional 29 radio components, 6 of which we believe are components of multi-component radio sources, and 23 of which were matched to faint SERVS sources below the catalog limit, resulting in an 87% match rate. Of the remaining unmatched objects, 134 (9%) were confused by brighter objects (mostly stars and bright galaxies) in SERVS. Of the remainder, only 31 (2%) appeared to be completely blank fields, and a further 28 were most likely blank, but were within $\approx 2''$ of faint objects in the field. These statistics emphasize the rarity of infrared-faint radio sources (Norris et al. 2011).

To evaluate the number of matches expected at random, we offset the positions of the radio sources by approximately 1 arcmin in R.A. and decl., and redid the matching four times with different offsets. The mean number of random matches was 90, corresponding to 6% of the number of radio components, which we treat as negligible.

[17] http://mattiavaccari.net/df

4. PHOTOMETRIC REDSHIFTS

4.1. Determination of Photometric Redshifts

Photometric redshifts of the objects observed in the SERVS study were obtained by J. Pforr et al. (2015, in preparation) using the Hyper-z photometric redshift code (Bonzella et al. 2000). A correlation of the photometric redshifts with the spectroscopic redshifts of AGNs in the field (see below) is described in the appendix, and shows that ~85% of the redshifts are accurate to within an rms of $\Delta z/(1+z) \approx 0.06$, the remainder being outliers. Highly luminous AGNs at high redshifts, where the hot dust from AGNs in the IRAC 3.6 and 4.5 μm bands can affect the redshift estimate, however, may have poorer photo-zs.

Of the photometric redshifts for the radio galaxies, 20 (1%) failed to find a solution. All of these failed solutions had only limits on their detection in either, or both, of the *J*-band or *K*-band. To ensure a good quality photometric redshift, we thus excluded the 254 objects (20% of the 1245 objects matched between the radio and SERVS) lacking a *J*- or *K*-band detection from any analysis that needed redshift information, ensuring that we had a minimum of four bands to estimate a redshift (*J*, *K*, [3.6], and [4.5]). In Figure 2, we show the 1.4 GHz flux density distribution of the survey for objects with and without photometric redshifts, indicating that there is not a very strong bias toward, for example, only the brighter radio sources having photometric redshift information. The photometric redshifts extend out to $z \approx 5$, as seen in Figure 3 (though some of the redshifts at $z > 4$ use only the minimum four bands, and thus may be unreliable). There is a dip in the redshift distribution at $z \approx 1.4$, which has no clear origin. Two possible explanations are that it may be a degeneracy in the photometric redshifts in the region of the "redshift desert" where the optical bands, in particular, do not contain strong spectral features to constrain the redshifts, or that it may reflect real large-scale structure in the field. Spectroscopic redshifts were available for 62 of the AGNs from Lacy et al. (2013) or the SDSS quasar survey (Ahn et al. 2014), including the normal type-1 AGN, whose optical emission is dominated by quasar light. We have used these in preference to the photometric redshifts where applicable.

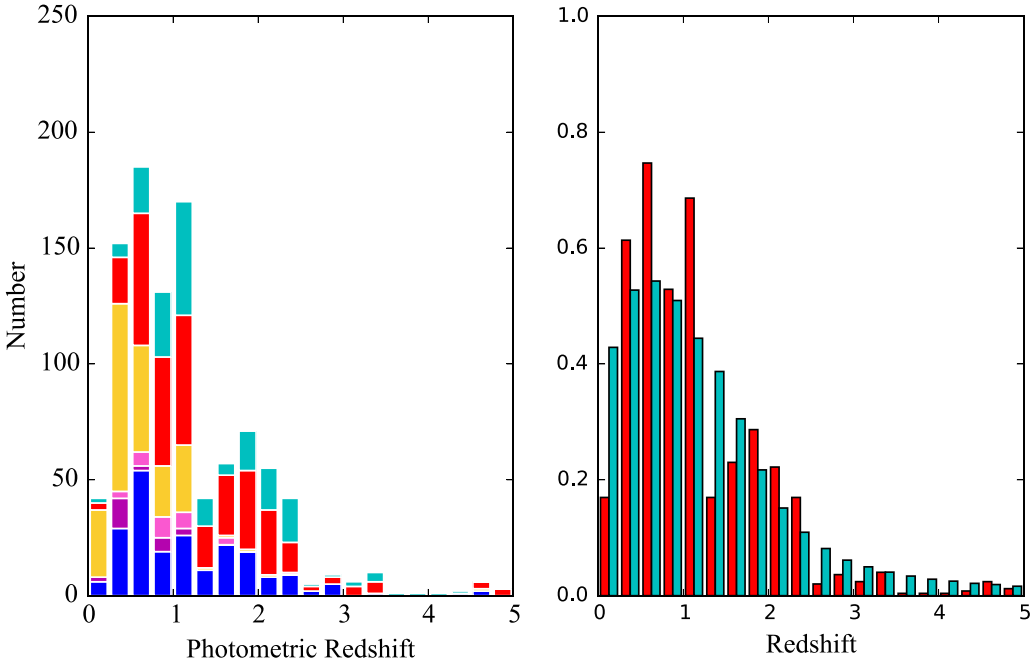

Figure 3. Left: photometric redshift distribution by type (see Section 5). Blue indicates actively accreting (cold mode) AGNs; dark magenta indicates hot-mode AGNs (based on the IRAC color–color plot); light magenta indicates likely hot-mode AGNs (based on q_{24}); red indicates ambiguous AGNs/star-forming objects; and cyan indicates unclassifiable objects. Right: the red histogram shows the normalized photometric redshift distribution for our sample, the cyan histogram shows the predicted redshift distribution from the full volume of the SKA simulations (Wilman et al. 2008).

4.2. Predictions of Photometric Redshifts for μJy Radio Sources

We used the SKA Simulated Skies (S^3) extragalactic model (Wilman et al. 2008) that uses measured luminosity functions combined with an underlying numerical dark matter simulation to obtain a predicted redshift distribution for μJy radio sources. This predicted redshift distribution is compared to our measured one in Figure 3. Both distributions peak at $z \approx 0.7$, though our measured distribution has fewer sources in the lowest redshift bin. This deficit is also seen in the smaller (but much more spectroscopically complete) sample of Simpson et al. (2012), and thus is unlikely to be due to large-scale structure fluctuations, though we cannot rule out incompleteness at very low redshifts due to galaxies being resolved out in the radio survey. We see fewer sources in the $z > 2.5$ bins than the predictions, though this may be explained by the 20% of faint sources we excluded due to missing *J*- and/or *K*-band detections. The median redshift we observe, 0.99, is very similar to the median redshift predicted by the simulations (1.04).

5. OBJECT CLASSIFICATION

We used a combination of a mid-infrared color–color diagram and the radio to mid-infrared flux ratio to classify as many of the radio sources as possible into three overall classes, namely cold-mode AGNs (high accretion rate objects with dynamically cold accretion flows and Eddington Luminosities $L_{\rm Edd} \sim 0.01$–1), hot-mode AGNs (low accretion rate objects accreting gas at about the galaxy virial temperature of $\sim 10^6$ K, with $L_{\rm Edd} \lesssim 0.01$, and jets possibly powered by the spin of the black hole, e.g., Martínez-Sansigre & Rawlings 2011) and star-forming galaxies. Mao et al. (2012) show that mid-infrared classifications are broadly consistent with those from spectrosopy.

5.1. Rapidly Accreting, Cold-mode AGNs

When looking for the relative contributions of AGNs and star-forming galaxies, bright AGNs are simpler to isolate than star-forming galaxies. For the 479 objects that were detected in all four of the 3.6, 4.5, 5.8, and 8.0 μm bands of the IRAC in the SWIRE data, we were able to isolate rapidly accreting, cold-mode AGNs using the method proposed by Lacy et al. 2004, 2007), which selects AGNs based on their color relative to star-forming or quiescent galaxies. Cold-mode AGNs have a characteristic red power law in the mid-infrared that stands out well in a $\log_{10}(S_{5.8}/S_{3.6})$ versus $\log_{10}(S_{8.0}/S_{4.5})$ color–color plot, (Figure 4, left). We used $S_{3.6}$ and $S_{4.5}$ from SERVS and $S_{5.8}$ and $S_{8.0}$ from SWIRE. Three cuts were made: $\log_{10}(S_{5.8}/S_{3.6}) > -0.1$, $\log_{10}(S_{8.0}/S_{4.5}) > -0.2$, and $\log_{10}(S_{8.0}/S_{4.5}) \leqslant 0.8 \log_{10}(S_{5.8}/S_{3.6})$, which produce the wedge-shaped area in the upper right corner of Figure 4. This area represents the objects likely to be cold-mode AGNs. These 226 objects make up 15% of the radio sources in the Ibar et al. survey (Figure 5). Spectroscopic follow-up of AGN samples selected in this manner show that this particular "wedge" selection is reliable in the sense that 78% (527 out of 672) of objects for which spectroscopic redshifts and classifications could be obtained using optical or near-infrared spectra are confirmed as AGNs (Lacy et al. 2013). (Many of the remainder may also be highly obscured AGNs, but cannot be confirmed as such from optical/near-infrared data alone.) Among the cold mode AGNs there are a total of six type-1 quasars from the Sloan Digital Sky Survey Data Release 10 (Ahn et al. 2014; five of which are in the Lacy et al. 2013 sample).

5.2. Low Accretion Rate, Hot-mode Radio AGNs

Lacy et al. (2006), Afonso et al. (2011), Gurkan et al. (2014), and Singh et al. (2014) also find that some weak radio AGNs appear outside the AGN or star-forming galaxy selection

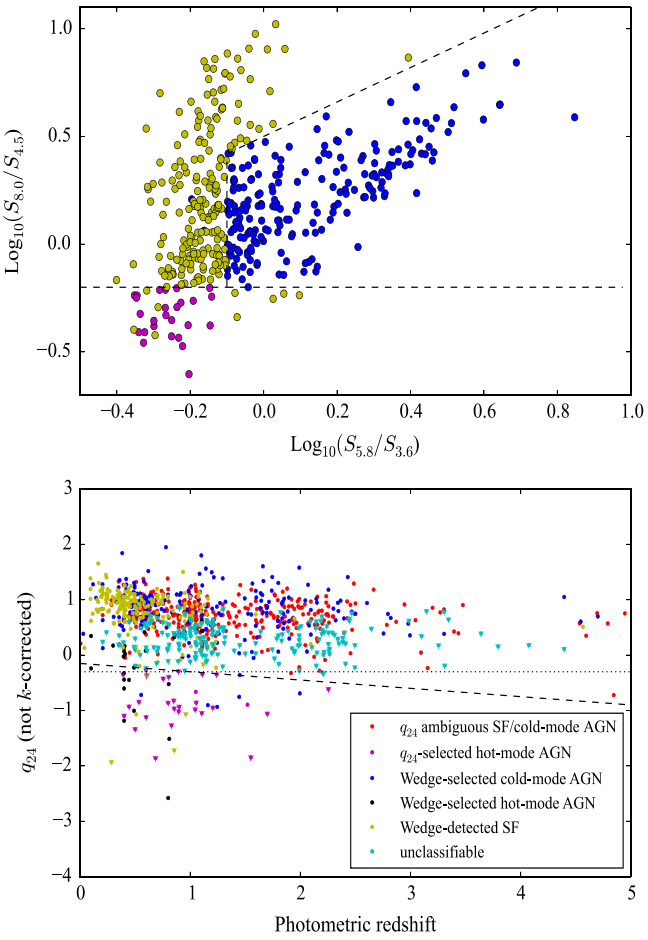

Figure 4. Classification of radio sources. Left: infrared color–color diagram. The four lines separate the objects into three areas: the wedge-shaped area in the upper right corner contains likely cold-mode AGNs (blue dots); the area occupying the lowest two corners contains likely hot-mode AGNs (black dots); and the area in the upper left corner contains likely star-forming galaxies (yellow dots). Note that there are a few objects classified as starbursts in the hot-mode AGN region, these are Herschel detections and are mostly $z > 1$ ULIRGs (see Section 5.5). Right: $q_{24} = \log_{10}(S_{24}/S_{1400})$ (not k-corrected) against redshift for the radio sources with matches at 24 μm in the SWIRE catalog. Downward pointing triangles indicate upper limits. The dashed line indicates the criteria we used to separate radio-loud hot-mode AGNs from cold-mode AGNs and starbursts for objects with photometric redshifts, the dotted line for those without (see the text for details).

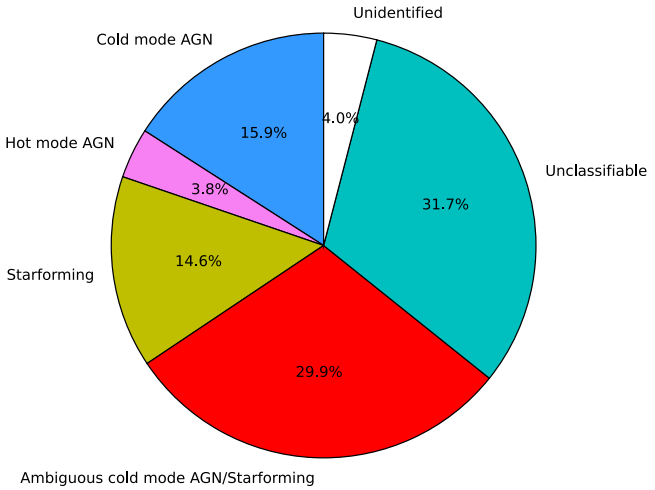

Figure 5. Pie chart for the whole Ibar et al. 1.4 GHz survey using our classifications described in Section 5. The number of objects in each class are as follows: 226 cold mode AGNs, including six type-1 quasars; 74 hot mode AGNs (comprising 37 from the four-band IRAC classification and 37 from the q_{24} classification); 207 star-forming galaxies; 437 objects ambiguous between star formation and cold-mode AGNs; 464 unclassifiable objects (excluding those that are definitely unidentified in SERVS), and 59 unidentified objects.

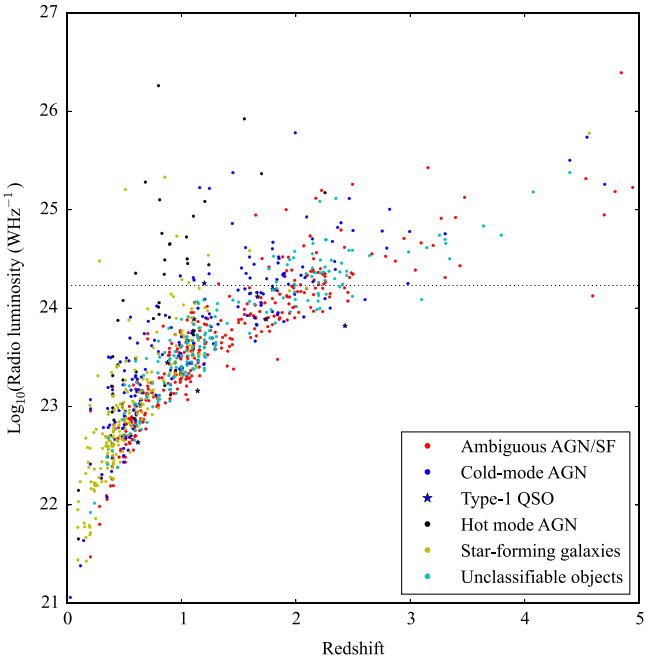

Figure 6. Radio luminosity vs. redshift for the radio sources, classified according to their mid-infrared properties. The dotted line indicates a radio luminosity from star formation of $1000 M_{\odot}$ yr^{-1}, close to the highest seen in starbursts (e.g., Karim et al. 2013) assuming a Salpeter IMF, objects with ambiguous AGN/SF classifications (red dots) above this line are most likely to be AGN-dominated. As discussed in Section 4.1, the majority of our redshifts are photometric, however, we include 62 spectroscopic redshifts.

region, with IRAC colors similar to quiescent galaxies. These galaxies are likely the low accretion rate, "hot mode" AGNs, whose radio jets are highly efficient. These radio sources can be found in the area beneath the cut formed by the line $\log_{10}(S_{8.0}/S_{4.5}) = -0.2$ in the left-hand panel of Figure 4.

We also use the $q_{24} = \log_{10}(S_{24}/S_{1400})$ value to classify objects without four-band IRAC detections (e.g., Ibar et al. 2008). As the SWIRE 24 μm flux density limit, $\approx$150 μJy, is five times $S_{1.4\,\mathrm{GHz}}$ of our faintest radio sources, and given that the typical value of q_{24} for star-forming galaxies is $\approx$1 (Appleton et al. 2004; Ibar et al. 2008), we expect to detect the majority of star-forming galaxies and cold-mode AGNs at 24 μm. We indeed find that the fraction of radio sources detected at 24 μm is high (overall, 874/1245 (70%) of matched radio sources are detected at 24 μm). Thus, the radio-bright objects not detected at 24 μm are likely to be hot-mode AGNs. We place the dividing line between radio-loud and radio-quiet at $q_{24} \approx 0$ at $z = 0$, then use the template k-corrections shown in Figure 1 of Ibar et al. (2008) to approximate the change in redshift of this dividing line as $q_{24} < -0.15(1 + z)$ (the dashed line in Figure 1, right-hand panel). For those objects not detected at 24 μm, we assume a limit of 150 μJy to classify them. We separate the hot mode AGNs selected using the wedge-based and q_{24}-based methods in Figures 3 and 4, but thereafter include them all in a single class, that comprises about 4% of the total radio source population in this sample.

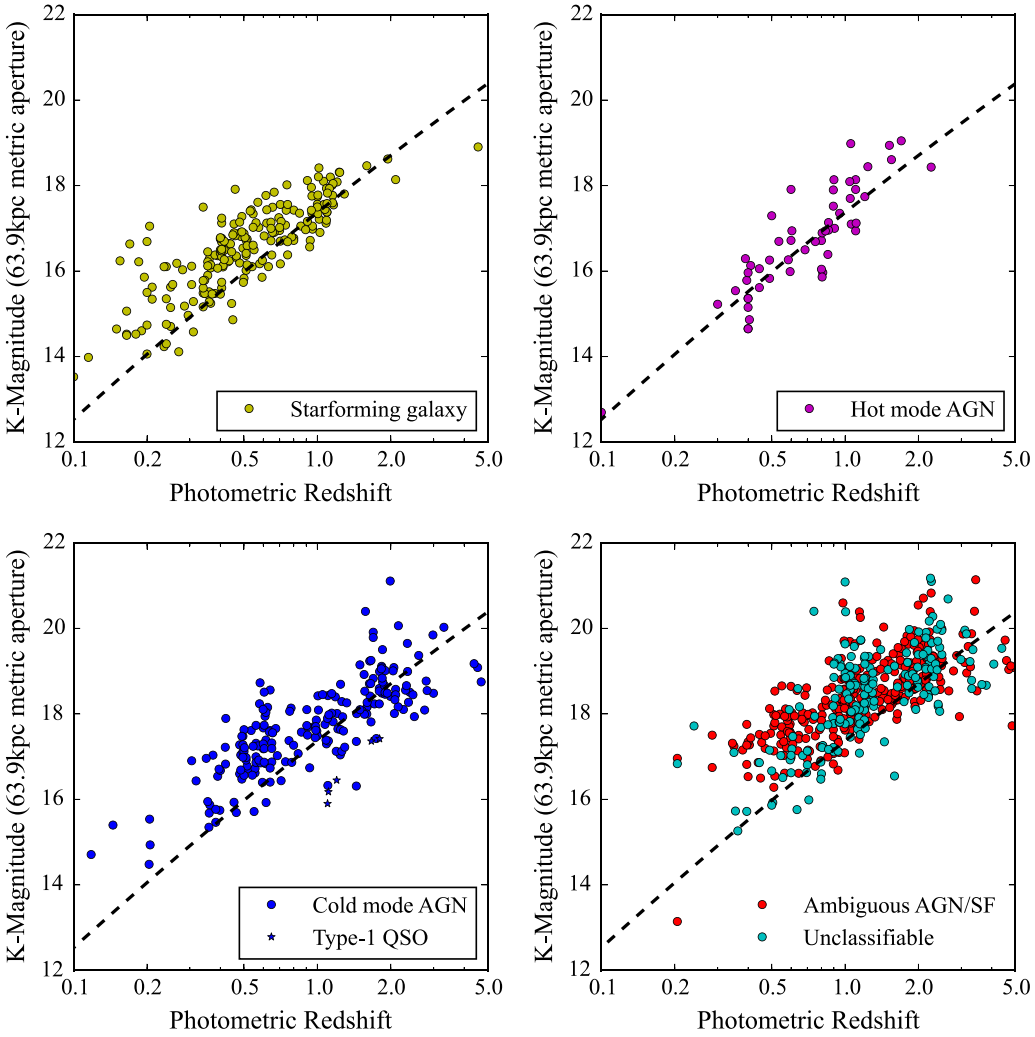

Figure 7. K–z relation, split by radio source type, as defined in Section 5. The dashed line indicates the K–z relation for radio sources from much brighter surveys, as defined by Willott et al. (2003). The hot-mode AGNs are the only class of object that appears to trace the same K–z relation as samples of radio sources selected from surveys ∼1000 times brighter in radio flux density.

For the objects lacking photometric redshifts, we approximated a classification by assuming a mean redshift of unity (dotted line in the right-hand panel of Figure 4). As can be seen, this should result in $\lesssim$10 misclassifications.

5.3. Star-forming Galaxies and 24 μm Detected Objects with Ambiguous Classifications

The remainder of the objects in the infrared color–color diagram—the upper left corner in Figure 4—correspond to star-forming galaxies, and make up 15% of the radio sources. In addition, 30% of objects are detected at 24 μm with q_{24} above the dashed (or dotted, in the case of objects lacking photometric redshifts) line in the right-hand panel of Figure 4, but not detected in all four IRAC bands. These most likely comprise a mix of cold-mode radio AGNs and star-forming galaxies, and we henceforth classify them as "ambiguous AGN/SF."

5.4. Unclassifiable Objects

32% percent of the identified radio sources remain unclassifiable using either the infrared color–color diagram or q_{24}, because they lack four-band IRAC detections, are undetected at 24 μm, and their flux density limit at 24 μm is insufficiently deep compared to their radio fluxes to classify them as radio-loud or radio-quiet.

5.5. Comparison of Wedge and q_{24} Selection

For the most part, our classification scheme is self-consistent between the wedge technique and the q_{24} one. Among the objects with spectroscopic redshifts, however, 15/37 of the hot mode AGNs that are classified as such by the wedge technique show up as radio-quiet in the q_{24} plot. Furthermore, in eight cases, objects initially classified as hot-mode AGNs are detected in Herschel HerMES (Oliver et al. 2012) images at 250 μm and also have photometric redshifts >1. These are most likely misclassified star-forming Ultraluminous Infrared Galaxies, which, due to their high redshifts, no longer have the PAH features in the IRAC 8 μm band resulting in them falling out of the star formation region in Figure 4 (left). They have been reclassified as star-forming galaxies. There is also one low redshift ($z = 0.04$) galaxy that appears to be a HerMES detection, we also reclassify it as a starburst. The remainder tend to plot in the radio-louder side of the infrared-radio correlation. They may

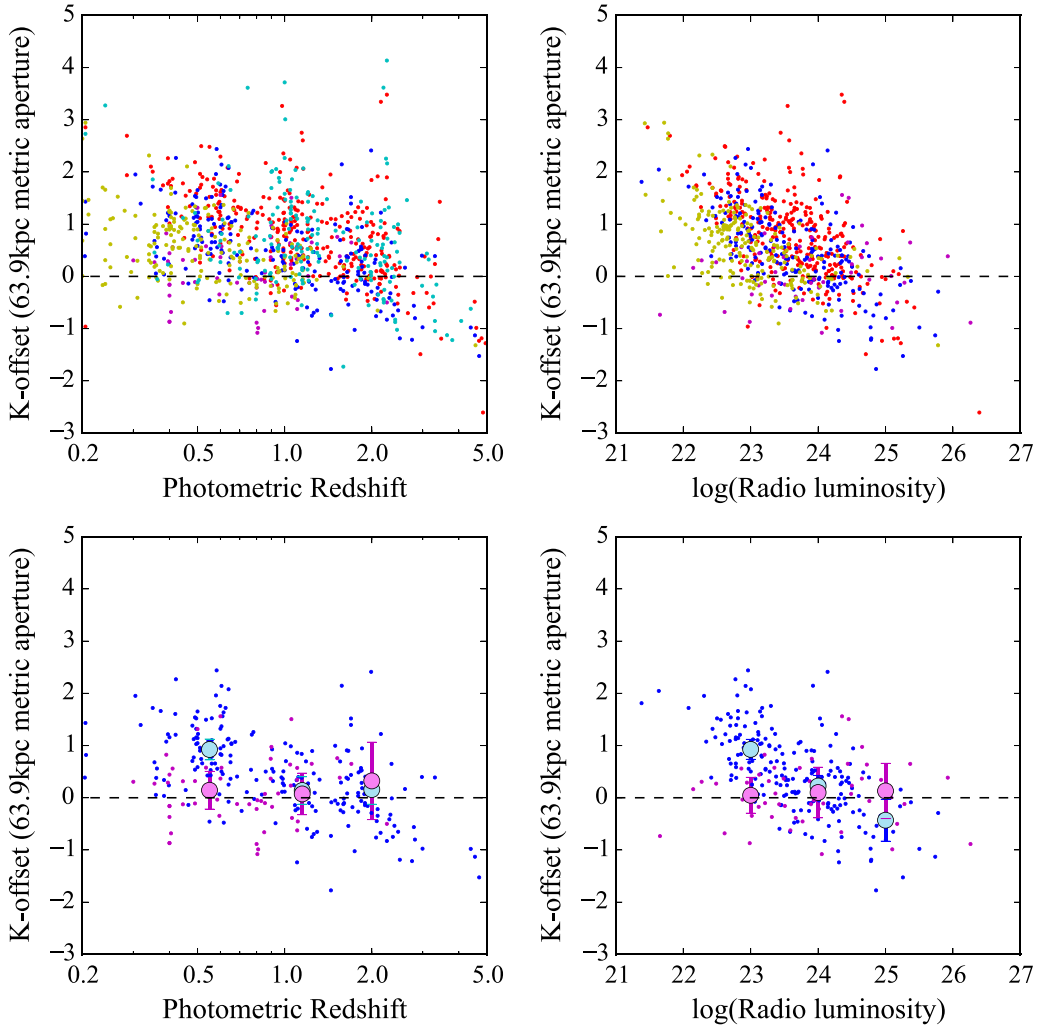

Figure 8. Offsets from the $K-z$ relation of Willott et al. (2003) as a function of redshift and radio luminosity (symbol colors as in Figure 4). Top panels: all radio source types. Bottom panels: AGN-powered radio sources only. The large gray and cyan points represent averages, with 3σ error bars, of the hot-mode and cold-mode AGNs, respectively.

have significant residual star formation, or 24 μm emission from their AGN (although hot-mode radio AGN tend to be faint in the mid-infrared, some do have significant mid-infrared emission, e.g., Ogle et al. 2005). Similarly, there are 4/207 galaxies classified as star-forming in the wedge selection that appear radio-loud in the q_{24} one, these may be radio-loud AGNs in starburst galaxies. Further, more accurate, classification could be attempted with full SED fitting, including *Herschel* data from the HerMES survey (Oliver et al. 2012), but we will defer this activity to a future paper.

Our classification results can be compared to the study of Bonzini et al. (2013), who used a survey of similar depth in the Extended Chandra Deep Field South to classify a sample of 883 radio sources as 19% radio-loud AGNs, 24% radio-quiet AGNs, and 57% star-forming galaxies. The main difference between our classification techniques and those used by Bonzini et al. is their use of a less conservative q_{24} criterion for defining radio-loud AGNs (called "hot mode" AGNs in this paper), and also their X-ray data and deeper *Spitzer* data that allows them to resolve more ambiguities between cold-mode AGNs and star-forming galaxies.

6. PROPERTIES OF RADIO SOURCES

6.1. Radio Luminosity and Spectral Index

In Figure 6, we plot the radio luminosity versus the photometric redshifts of the radio sources. The radio luminosity was calculated for objects within the μJy population using the flux densities and spectral indices of the 1.4 GHz objects within the Ibar et al. (2009) survey. Most of our radio sources have $L_{1.4} \sim 10^{22.5}$–$10^{24.5}$ WHz^{-1}, spanning the traditional boundary in luminosity between radio-loud and radio-quiet objects. With few exceptions (probably misclassifications) all the star-forming galaxies selected via Figure 1 have $L_{1.4} < 10^{24.5}$ WHz^{-1}, corresponding to star formation rates $\lesssim$2000 $M_{\odot}$yr^{-1}, assuming a Salpeter IMF.

The Ibar et al. catalog includes spectral indices between 610 MHz and 1400 MHz (α_{1400}^{610}) for objects detected at both frequencies. The mean α_{1400}^{610} for the objects matched to SERVS is -0.78. The mean spectral indices for the cold-mode AGNs and star-forming galaxies are very similar to the overall mean (-0.77 and -0.79, respectively). That for the hot-mode AGNs is significantly flatter, -0.44, indicating a large fraction of flat-spectrum AGNs in that class.

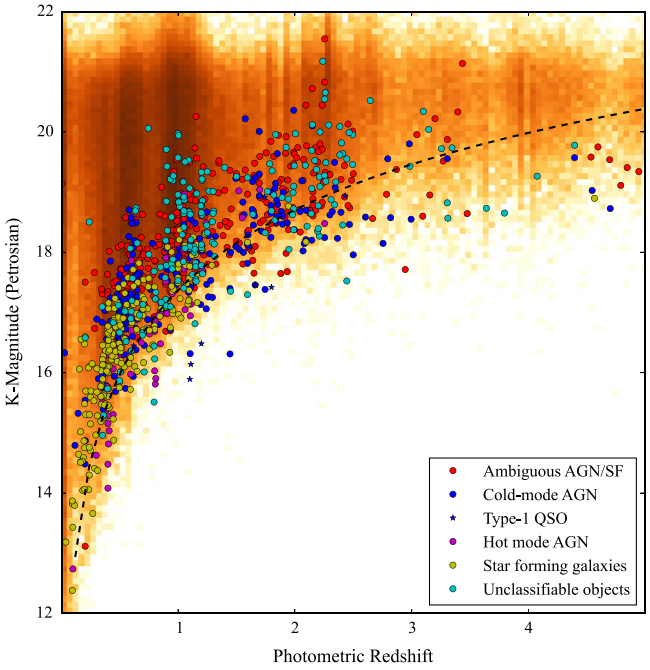

Figure 9. K–z relation by type for the radio sources, with the overall K-magnitude distribution for the SERVS-Lockman data fusion catalog shown as a log-scaled density field. Symbols are the same as in Figure 3. The K–z relation from Willott et al. (2003) is shown as the dashed line.

6.2. K-band Emission

K-band emission from radio galaxies tends to consist primarily of stellar light (Lacy et al. 1995; Best et al. 1998; Simpson et al. 1999; Seymour et al. 2007), though in very luminous cold-mode AGNs there can be significant contributions from reddened quasar continuum (Rawlings et al. 1995) or emission lines (Eales & Rawlings 1993). Previous results generally found that the K–z relation corresponded to a curve representing a stellar population that formed its stars at very high redshifts ($z > 5$) and passively evolved afterward (e.g., Lacy et al. 2000; Jarvis et al. 2001; Willott et al. 2003). In Figure 7, we plot the K-magnitudes against the logarithms of their photometric redshifts. The dashed curve in Figure 7, which has a function of $K = 17.37 + 4.53\log_{10}(z) - 0.31(\log_{10}(z))^2$, was proposed by Willott et al. (2003) as the polynomial of best fit for luminous steep-spectrum radio galaxies within a standard 63.9 kpc metric aperture. Willott et al. show that their K–z relation fit closest to a model in which most stars formed in a single burst at redshifts of $z = 10$, and evolved passively afterward. However, the scatter toward brighter magnitudes at $z > 2$ apparent in both Willott et al. and in Figure 7 cannot eliminate a model in which many radio source hosts formed at a lower redshift, $z \sim 5$. This is discussed further in Section 6.3 below.

Figure 7 shows that most of the hosts of μJy radio sources are fainter in the K-band than the mean for the hosts of the much radio-brighter sources from the 3C, 6C, and 7C samples (with typical radio flux densities at 1.4 GHz ~50–1000 mJy) studied by Willott et al. (2003). This is perhaps not surprising for the star-forming galaxy population, which has a very different physical mechanism for radio emission than the AGN populations that dominate the Willott et al. sample, but it also seems true for the cold-mode AGN population, at least at low redshifts/luminosities (see also Barger et al. 2014). In Figure 8, we plot the offset from the K–z relation for different types of objects (especially AGNs) as a function of radio luminosity and redshift. In the lowest radio luminosity bin, $10^{22.5-23.5}$ WHz^{-1}, the mean and error in the mean of the offset is 0.93 ± 0.06 for cold-mode AGNs (significant at 15σ), but insignificant (0.05 ± 0.11) for hot-mode AGNs. In the next bin, $10^{23.5-24.5}$ WHz^{-1}, the offsets are barely significant (0.22 ± 0.07) for the cold-mode AGNs and again insignificant (0.10 ± 0.16) for the hot-mode AGNs, and, similarly, we see no significant offsets in the highest luminosity bin ($10^{23.5-24.5}$ WHz^{-1}).

Figure 9 shows the Petrosian magnitudes[18] of the radio sources overlaid on the K–z distribution from the entirety of the SERVS Fusion catalog, including optical and infrared sources which were not matched to radio sources. Despite the offset from the K–z relation for the most luminous radio galaxies that we observe, the radio matched objects are, at any given redshift, among the most luminous objects, and are generally much more luminous than the objects found only in the optical, infrared, or ultraviolet surveys.

6.3. Stellar Mass

We estimated the approximate stellar masses of the Lockman Hole radio sources using the 3.6 μm flux density and a 1.4 Gyr stellar population template from Bruzual & Charlot (2003) to calculate the rest-frame K-band luminosity, L_K. The 3.6 μm wavelength is a good compromise between being close to rest-frame K-band at $z \sim 1$, while at the same time not usually containing significant contamination from hot dust emission from the AGNs (Caputi 2013). The choice of stellar population template makes only a small difference to the k-corrections in the near-infrared. We then used K-band mass-to-light ratio estimates at $z = 0$–1 from Drory et al. (2004) and at $z \sim 2$ from Borys et al. (2005) to parameterize the evolution of the K-band mass-to-light ratio in a typical massive galaxy as $M/L_K \approx 1.0/(1 + 1.5z)$. The result is shown in Figure 10. Some of the largest indicated masses for the cold-mode accretion AGNs are probably spurious, produced by contamination of the 3.6 μm flux density by AGN hot dust emission. For the remainder, we see a fairly well-defined cutoff at $\sim 10^{11.5}\,M_\odot$.

We further estimated the stellar masses of the optical and infrared sources that were not matched to radio sources, plotting the distribution of stellar masses of the radio-loud ($L_{1.4\,\mathrm{GHz}} > 10^{24}$ WHz^{-1}) and radio-quiet populations in Figure 9. This figure shows that the radio-loud sources tend to be among the objects with the largest stellar masses at any redshift (see also Bonzini et al. (2013), who find that the radio-loud AGNs in their work are also in host galaxies significantly more massive than cold-mode AGN or star-forming galaxies), though the distribution of masses of our "hot mode" AGNs lacks the tail to low masses (below $\approx 10^{10.5}\,M_\odot$ seen in Figure 9 of Bonzini et al.). A high mean mass for the radio-loud population is expected, based on the work of Best et al. (2005) and Simpson et al. (2012).

Effective AGN feedback depends on a high duty cycle of activity (Croton et al. 2006), so a high fraction of radio-loud AGNs is needed if radio-jet powered AGN feedback models are to be plausible. Among objects with stellar masses greater than or equal to $10^{11.5}\,M_\odot$ with redshifts $0.5 < z < 2.5$, we

[18] Petrosian magnitudes include the light out to a radius where the surface brightness of the galaxy falls to 0.2 of its mean value within that aperture.

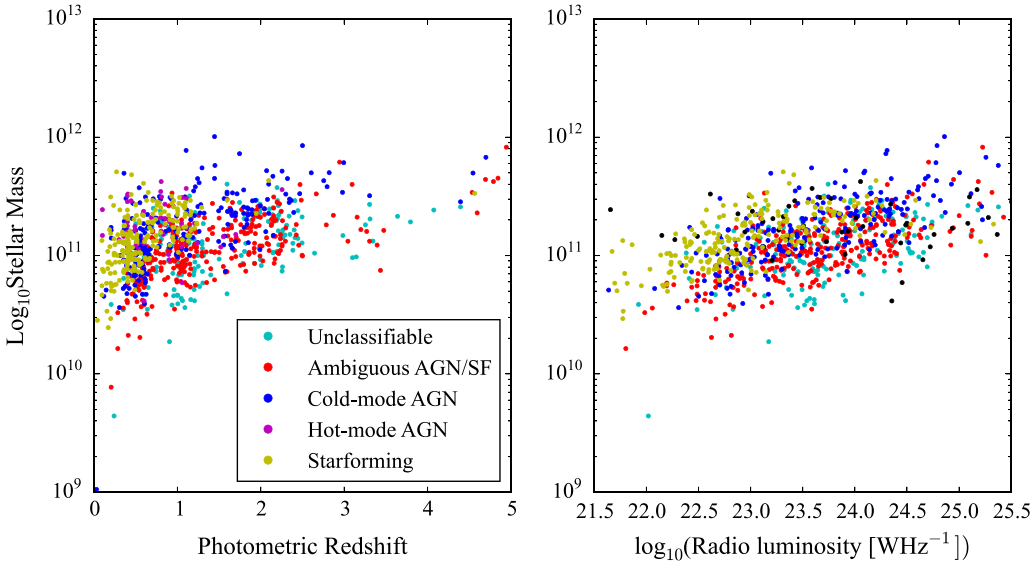

Figure 10. Stellar masses of the radio sources as a function of (left) redshift and (right) radio luminosity.

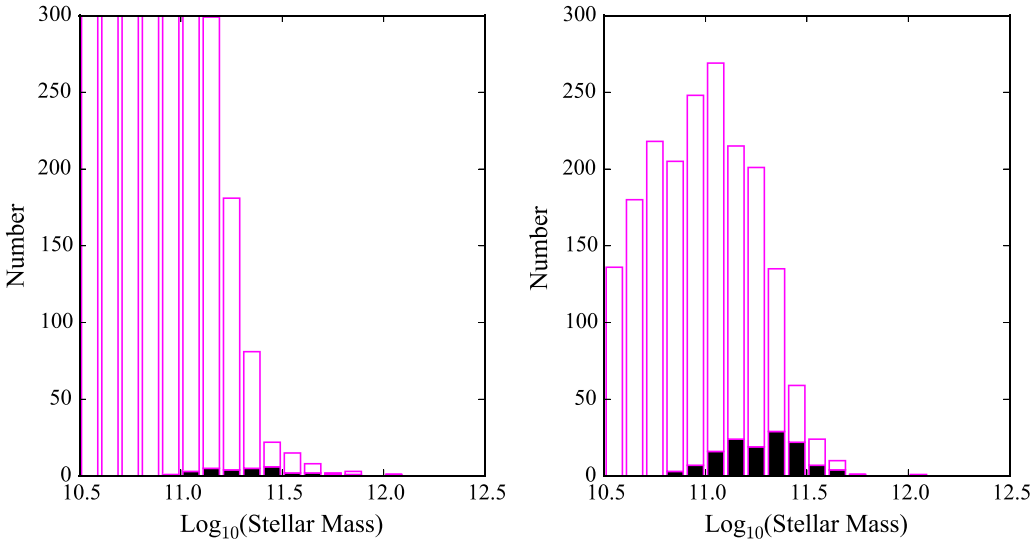

Figure 11. Histograms of stellar masses, radio-quiet objects shown in magenta, radio-loud objects in black. The left panel is for objects with $0.5 < z < 1.5$, the right panel for objects with $1.5 < z < 2.5$.

found 19/69, or 28%, of all massive galaxies are radio-loud (Figure 11), consistent with this requirement. At $z > 2.5$, the space density of galaxies with masses $\sim 10^{11.5} M_{\odot}$ is very low, $\sim 10^{-6}$ Mpc^{-3} (Duncan et al. 2014), and remains similar to the space density of radio sources. It is thus quite plausible that, when a galaxy (and its black hole) reaches a certain critical mass, it is able to switch on as a radio-loud object with a duty cycle of a few tens of percent. Better statistics are needed at high-z, however, both on the radio source population and on the numbers of massive galaxies to understand the evolution of radio source hosts at the earliest epochs.

The star-forming galaxies also have relatively high stellar masses, $\sim 10^{11}\, M_{\odot}$. The most likely explanation for this is that these star-forming galaxies are at the high end of the radio luminosity function for star-forming objects, with typical radio luminosities $\sim 10^{22.5}$ WHz^{-1}, forming stars at rates of $\sim 10\, M_{\odot}$ yr^{-1} (Chabrier IMF; Karim et al. 2011). Karim et al. (2011) and Zwart et al. (2014) show that, at the redshifts at which these objects are mostly seen in our study ($z \sim 0.3-0.5$), these objects have a typical specific star formation rate SSFR ~ 0.1 Gyr^{-1}. Although less massive objects tend to have higher SSFR, the trend is relatively weak, therefore, fewer massive galaxies would be expected to have lower absolute star formation rates and thus would be missing from the survey.

7. CONCLUSIONS

The results presented in this paper include one of the first estimates of the redshift distribution and K–z relation for a survey with a large fraction of radio sources <100 μJy. The redshift distribution we find features a median value of $z \approx 1$ and a tail out to redshifts of $z \approx 5$. This is not entirely consistent with the predicted redshift distribution of μJy radio sources from the S^3 simulations, which suggests a larger fraction of sources at $z < 0.25$, though the median redshift is

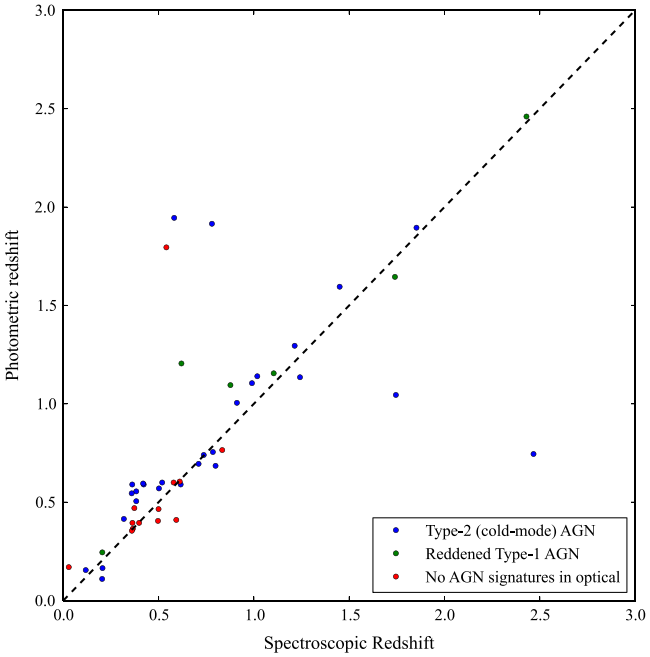

Figure 12. Photometric redshift vs. spectroscopic redshifts for the objects in the sample of Lacy et al. (2013) with type-2, red type-1 or non-AGN optical/near-infrared spectra and reliable redshifts.

very similar, and issues of over-resolution in the radio may explain the apparent deficit of very-low-z sources.

The galaxies detected in the deep radio survey at μJy levels tend to be more luminous in the K band than objects that were not detected in the radio survey. Nevertheless, we see evidence that the K–z relation is breaking down, not only due to the increased fraction of star-forming galaxies, but also because the cold mode AGN radio sources with 1.4 GHz radio luminosities $L_{1.4} \lesssim 10^{24}$ WHz^{-1} tend to exist in less luminous host galaxies. Thus, lower luminosity radio sources are no longer found in only the most massive galaxies, and so, as Simpson et al. (2012) point out, the K–z relation defined for powerful radio sources should not be used for estimating redshifts in μJy surveys. It is possible that the $L_{1.4} \lesssim 10^{24}$ WHz^{-1} cold-mode AGNs have a different mechanism for producing radio emission rather than AGN jets. Star formation (Kimball et al. 2011) or synchrotron emission powered by shocks in thermal outflows (Zakamska & Greene 2014) have been suggested as possible alternate mechanisms that dominate over jet powered radio emission at lower luminosities. Hot mode AGNs, on the other hand, continue to be found in only the most massive galaxies at $L_{1.4} < 10^{24}$ WHz^{-1} and most likely continue to be powered by jets. This picture is consistent with only the most massive galaxies containing black holes that are capable of producing the most powerful radio jets, and thus with a strong dependence of jet luminosity on black hole mass among AGNs (e.g., Laor 2000; Lacy et al. 2001; Kratzer & Richards 2014). We show that the fraction of massive galaxies that are radio-loud continues to be high (up to ≈30%) out to $z \sim 2$, a prerequisite for models where feedback from radio jets is able to limit star formation in their host galaxies, extending the results of Best et al. (2005) and Simpson et al. (2013).

We thank the referee for a careful reading of the manuscript. The National Radio Astronomy Observatory is a facility of the National Science Foundation operated under cooperative agreement by Associated Universities, Inc. This work made extensive use of TOPCAT (Taylor 2005) for catalog matching and analysis, and the Virtual Observatory SAMP protocol for communication between applications. This paper also made use of the SERVS Lockman data holdings in the Infrared Science Archive, ADS/IRSA.Atlas#2014/1025/091233_11822. J.A. gratefully acknowledges support from the Science and Technology Foundation (FCT, Portugal) through the research grant PTDC/FIS-AST/2194/2012 and PEst-OE/FIS/UI2751/2014.

APPENDIX
ACCURACY OF THE PHOTOMETRIC REDSHIFTS

Spectroscopic redshifts for some of the AGNs in this field were obtained by Lacy et al. (2013). We selected all 53 of the type-2, red type-1 (defined in Lacy et al. 2013 as having broad emission lines, but optical colors redder than normal quasars) and "non-AGN" objects (i.e. AGN candidates selected in the mid-infrared, but which showed no AGN signatures in their optical spectra) in common with the two samples, with spectroscopic redshift quality $q = 1$ in Lacy et al. (2013). The plot of spectroscopic versus photometric redshift is shown in Figure 12. The two sets of redshifts agree well, though the increasing dominance of the AGN component in the higher luminosity AGN above $z \approx 1$ introduces more scatter at high redshifts, and may also be responsible for some of the catastrophic outliers (15% of the matched objects). The scatter $\Delta z/(1+z) \approx 0.06$, though there is a small offset for the type-2 objects of $z_{\rm phot} - z_{\rm spec} \approx 0.15$ around $z = 0.4$, probably due to emission line contamination of broadband magnitudes. The type-2 objects in this plot are among the most infrared-luminous of the "cold-mode" AGNs in this paper, and thus will be the most prone to contamination by AGN flux in the near-infrared.

REFERENCES

Afonso, J., Bizzocchi, L., Ibar, E., et al. 2011, ApJ, 743, 122
Afonso, J., Georgakakis, A., Almeida, C., et al. 2005, ApJ, 624, 135
Ahn, C. P., Alexandroff, R., Prieto, C. A., et al. 2014, ApJS, 211, 17
Appleton, P. N., Fadda, D. T., Marleau, F. R., et al. 2004, ApJS, 154, 147
Barger, A. J., Cowie, L. L., Chen, C.-C., et al. 2014, ApJ, 784, 9
Bertin, E., & Arnouts, S. 1996, A&AS, 117, 393
Best, P. N., Kauffmann, G., Heckman, T. M., et al. 2005, MNRAS, 362, 25
Best, P. N., Longair, M. N., & Röttgering, H. J. A. 1998, MNRAS, 295, 549
Bonzella, M., Miralles, J.-M., & Pello, R. 2000, A&A, 363, 476
Bonzini, M., Padovani, P., Mainieri, V., et al. 2013, MNRAS, 436, 3759
Borys, C., Smail, I., Chapman, S. C., et al. 2005, ApJ, 635, 853
Bruzual, G., & Charlot, S. 2003, MNRAS, 344, 1000
Caputi, K. I. 2013, ApJ, 768, 103
Condon, J. J. 1992, ARA&A, 30, 575
Croton, D. J., Springel, V., White, S. D. M., et al. 2006, MNRAS, 365, 11
Drory, N., Bender, R., & Hopp, U. 2004, ApJL, 616, L103
Duncan, K., Conselice, C. J., Mortlock, A., et al. 2014, MNRAS, 444, 2960
Eales, S. A., & Rawlings, S. 1993, ApJ, 411, 67
Ferramacho, L. D., Santos, M. G., Jarvis, M. J., & Camera, S. 2014, MNRAS, 442, 2511
González-Solares, E. A., Irwin, M., McMahon, R. G., et al. 2011, MNRAS, 416, 927
Gurkan, G., Hardcastle, M. J., & Jarvis, M. J. 2014, MNRAS, 438, 1149
Huynh, M. T., Jackson, C. A., Norris, R., & Fernandez-Soto, A. 2008, AJ, 135, 2470
Ibar, E., Cirasuolo, M., Ivison, R., et al. 2008, MNRAS, 386, 953
Ibar, E., Ivison, R. J., Biggs, A. D., Lal, D. V., Best, P. N., & Green, D. A. 2009, MNRAS, 397, 281
Jarvis, M. J., & Rawlings, S. 2004, NewAR, 48, 1173
Jarvis, M. J., Rawlings, S., Eales, S., et al. 2001, MNRAS, 326, 1585
Karim, A., Schinnerer, E., Martínez-Sansigre, A., et al. 2011, ApJ, 730, 61

Karim, A., Swinbank, A. M., Hodge, J. A., et al. 2013, MNRAS, 432, 2
Kimball, A., Kellerman, K. I., Condon, J. J., Ivezić, Z., & Perley, R. A. 2011, ApJL, 739, L29
Kratzer, R. M., & Richards, G. T. 2015, AJ, 149, 61
Lacy, M., Bunker, A. J., & Ridgway, S. E. 2000, AJ, 120, 68
Lacy, M., Laurent-Muehleisen, S. A., Ridgway, S. E., et al. 2001, ApJ, 551, 17
Lacy, M., Petric, A. O., & Sajina, A. 2007, AJ, 133, 186
Lacy, M., Rawlings, S., Eales, S., & Dunlop, J. S. 1995, MNRAS, 273, 821
Lacy, M., Ridgway, S. E., Gates, E. L., et al. 2013, ApJS, 208, 24
Lacy, M., Sajina, A., Gates, E. L. & XFLS Team 2006, AN, 327, 258
Lacy, M., Storrie-Lombardi, L. J., Sajina, A., et al. 2004, ApJS, 154, 166
Laor, A. 2000, ApJL, 543, L111
Lawrence, A., Warren, S. J., Almaini, O., et al. 2007, MNRAS, 379, 1599
Lilly, S. J. 1989, ApJ, 340, 77
Lilly, S. J., & Longair, M. S. 1984, MNRAS, 211, 833
Lonsdale, C., Smith, H. E., Rowan-Robinson, M., et al. 2003, PASP, 115, 897
Mao, M. Y., Sharp, R., Norris, R. P., et al. 2012, MNRAS, 426, 3334
Martínez-Sansigre, A., & Rawlings, S. 2011, MNRAS, 414, 1937
Mauduit, J.-C., Lacy, M., Farrah, D., et al. 2012, PASP, 124, 1135
McLure, R. J., Willott, C. J., Jarvis, M. J., et al. 2004, MNRAS, 351, 347
Mignano, A., Prandoni, I., Gregorini, L., et al. 2008, A&A, 477, 459
Norris, R. P., Afonso, J., Cava, A., et al. 2011, ApJ, 736, 55
Ogle, P., Whysong, D., & Antonucci, R. 2005, ApJ, 647, 161
Oliver, S. J., Bock, J., Altieri, B., et al. 2012, MNRAS, 424, 1614
Owen, F. N., Morrison, G. E., Klimek, M. D., & Greisen, E. W. 2009, AJ, 137, 4846
Padovani, P., Bonzini, M., & Kellermann, K. I. 2015, MNRAS, 452, 1263
Padovani, P., Miller, N., Kellermann, K. I., et al. 2011, ApJ, 740, 20
Rawlings, S., Lacy, M., Sivia, D. S., & Eales, S. A. 1995, MNRAS, 274, 428
Seymour, N., Stern, D., de Breuck, C., et al. 2007, ApJS, 171, 353
Seymour, N., Dwelly, T., Moss, D., et al. 2008, MNRAS, 386, 1695
Simpson, C., Martínez-Sansigre, A., Rawlings, S., et al. 2006, MNRAS, 372, 741
Simpson, C., Rawlings, S., Ivison, R., et al. 2012, MNRAS, 421, 3060
Simpson, C., Rawlings, S., & Lacy, M. 1999, MNRAS, 306, 828
Simpson, C., Westoby, P., Arumugam, V., et al. 2013, MNRAS, 433, 2647
Singh, V., Beelen, A., Wadadekar, Y., et al. 2014, A&A, 569, 52
Smolčić, V., Padovani, P., Delhaize, J., et al. 2015, in Proc. AASKA14, in press (arXiv:1501.04820)
Smolčić, V., Schinnerer, E., Scodeggio, M., et al. 2008, ApJS, 177, 14
Strazzullo, V., Pannella, M., Owen, F. N., et al. 2010, ApJ, 714, 1305
Taylor, M. B. 2005, adass XIV, 347, 29
White, G. J., Hatsukade, B., Pearson, C., et al. 2012, MNRAS, 427, 1830
Willott, C. J., Rawlings, S., Blundell, K. M., et al. 2003, MNRAS, 335, 1120
Wilman, R. J., Miller, L., Jarvis, M. J., et al. 2008, MNRAS, 388, 1335
Zakamska, N. L., & Greene, J. E. 2014, MNRAS, 442, 784
Zwart, J. T. L., Jarvis, M. J., Deane, R. P., et al. 2014, MNRAS, 439, 1459